doi:10.1038/nature03571



NATURE 3571—6/5/2005—VBICKNELL—148660



# Genome-wide analysis of human kinases in clathrin- and caveolae/raft-mediated endocytosis

Lucas Pelkmans[1], Eugenio Fava[2], Hannes Grabner[2], Michael Hannus[4], Bianca Habermann[1,3], Eberhard Krausz[2] & Marino Zerial[1]

**Endocytosis is a key cellular process, encompassing different entry routes and endocytic compartments. To what extent endocytosis is subjected to high-order regulation by the cellular signalling machinery remains unclear. Using high-throughput RNA interference and automated image analysis, we explored the function of human kinases in two principal types of endocytosis: clathrin- and caveolae/raft-mediated endocytosis. We monitored this through infection of vesicular stomatitis virus, simian virus 40 and transferrin trafficking, and also through cell proliferation and apoptosis assays. Here we show that a high number of kinases are involved in endocytosis, and that each endocytic route is regulated by a specific kinase subset. Notably, one group of kinases exerted opposite effects on the two endocytic routes, suggesting coordinate regulation. Our analysis demonstrates that signalling functions such as those controlling cell adhesion, growth and proliferation, are built into the machinery of endocytosis to a much higher degree than previously recognized.**

Endocytosis supports a wide range of cellular functions, including nutrient uptake, downregulation of growth factors, cell-surface homeostasis, synaptic transmission and pathogen defence. Regulation of endocytic pathways is tightly coupled to the ability of cells to recognize, respond and adapt to extracellular stimuli. Different endocytic uptake mechanisms, including clathrin-mediated endocytosis (CME), caveolae/raft-mediated endocytosis, macropinocytosis and transactions between endosomes[1], are not only regulated by signalling molecules but also themselves contribute to signal transduction mechanisms[2–4]. A detailed understanding of these multifaceted processes would benefit from a comprehensive analysis of the components necessary for endocytic transport and their responses to physiological stimuli, which is now possible owing to the availability of genomic sequences[5]. We reasoned that an important first step in understanding the supra-molecular regulation of endocytosis was to explore the role of the human kinome (the genomic collection of human protein, lipid and carbohydrate kinases) in endocytosis[6]. Only a small number of protein kinases have so far been implicated in endocytic transport[1,7–9]. Here we undertook a genomic approach, systematically silencing predicted human kinases by RNA interference (RNAi), and determining the consequences of this silencing on two endocytic entry routes.

## High-throughput viral entry screens

Endocytic transport is a multi-step process consisting of ligand binding and sequestration into internalization sites, the formation, transport, tethering and fusion of endocytic carriers with endosomal compartments, the sorting of cargo, and cargo distribution to its final destination[1,10]. To identify genes regulating these events, we exploited two viruses that hijack the endocytic pathway to infect host cells[11,12], because virus infection is efficient, reproducible and easily measurable. Vesicular stomatitis virus (VSV) enters cells via clathrin-mediated endocytosis into early and late endosomes[13]. Simian virus 40 (SV40) is transported to the endoplasmic reticulum (ER)[14] upon caveolae-mediated endocytosis via caveosomes[15–17], as well as by non-caveolar, lipid raft-mediated endocytosis[18]. Notably, the same endocytic routes collectively regulate the signalling response of growth factor–receptor complexes[4,19–21].

The screening was performed using HeLa cells because their genes can be efficiently silenced with short interfering (si)RNA[22]. Three days after transfection (90% transfection efficiency and >70% reduction in messenger RNA), separate HeLa cell populations were infected with the two viruses using a low multiplicity of infection (MOI 0.1), to detect both reductions and increases in infection. As proof of principle (Supplementary Fig. S1a), we verified that VSV infection was specifically reduced by the silencing of established endocytic regulators like clathrin heavy chain and early endosome antigen 1 (EEA1; refs 23, 24), that SV40 infection was reduced by silencing of filamin and ceramide-glucosyl-transferase[25,26], and that both were reduced by ablation of *N*-ethylmaleimide sensitive factor (NSF)[27]. The partial (40%) inhibition of SV40 infection observed upon silencing of caveolin-1 (Cav1) indeed reflects virus entry via a caveolin- and clathrin-independent, but lipid raft-dependent mechanism[18,28].

## Genome-wide functional analysis of human kinases

The average relative infection index (RII, the ratio of infected siRNA-treated cells to infected control-treated cells) of VSV and SV40 was consistently reduced at least threefold by (1) silencing of the aforementioned genes, (2) using established inhibitors like GTPase-deficient dynamin2 (dynamin2-K44A), or (3) using methods such as endosomal pH neutralization ($NH_4Cl$), cytosol acidification (chlorpromazine) or cholesterol depletion (nystatin/progesterone) (RII $\leq$ 0.33, Fig. 1a and Supplementary Fig. S1a). We set this value

[1]Max Planck Institute of Molecular Cell Biology and Genetics,{#,46]. [2]MPI-CBG High-Throughput Technology Development Studio (HT-TDS), and{#,46]. [3]Scionics Computer Innovation GmbH, Pfotenhauerstrasse 108, 01307 Dresden, Germany. [4]Cenix Bioscience GmbH, Tatzberg 47, 01307 Dresden, Germany.

NATURE 3571—6/5/2005—VBICKNELL—148660

(RII ≤ 0.33) as the threshold for scoring inhibition, to identify necessary components or activators of the pathway. An RII greater than or equal to 3.00 was used as the threshold for scoring enhancement (RII ≥ 3.00), indicating a repressor of the pathway. A kinase was assigned as being involved in both clathrin- and caveolae-mediated endocytosis pathways if both RIIs were <0.4 or >2.50. Importantly, all RII values selected by these criteria fell outside the intervals defined by 3 s.d. of a large series of negative controls (Fig. 1a). See Supplementary Table S1 for a complete list of kinases and silencing phenotypes.

Out of the 590 human kinases screened (including lipid, protein, carbohydrate and hypothetical kinases), we identified a large number (208) as being involved in the two infectious entry routes. Whereas VSV infection was typically reduced, SV40 infection was enhanced for about half of the kinases. With the exception of CDK2 and GAK/auxillin, the kinases previously implicated in endocytosis (AAK1, Lck, c-Src, GSK3b, protein kinase C (PKC) isoforms and CK2) were represented, showing that the screen identified the expected genes.

A number of control tests were used to verify that the high number of hits reflected a prominent regulatory role for the kinome in the infectious entry routes, rather than promiscuity of the assays. First, silencing of 50 randomly selected genes (see Supplementary Table S2) yielded only one hit (*OXCT1*, Fig. 1b), suggesting that the kinome is specifically enriched in regulators of the two infectious routes. Second, mRNA from 72% of the whole kinome and at least 90% of the hits could be detected in untreated HeLa cells, indicating that most of the kinase genes selected are expressed in HeLa cells. Third, we addressed kinome-wide the effects on cell proliferation and apoptosis (Fig. 1a). Although silencing of some genes reduced cell

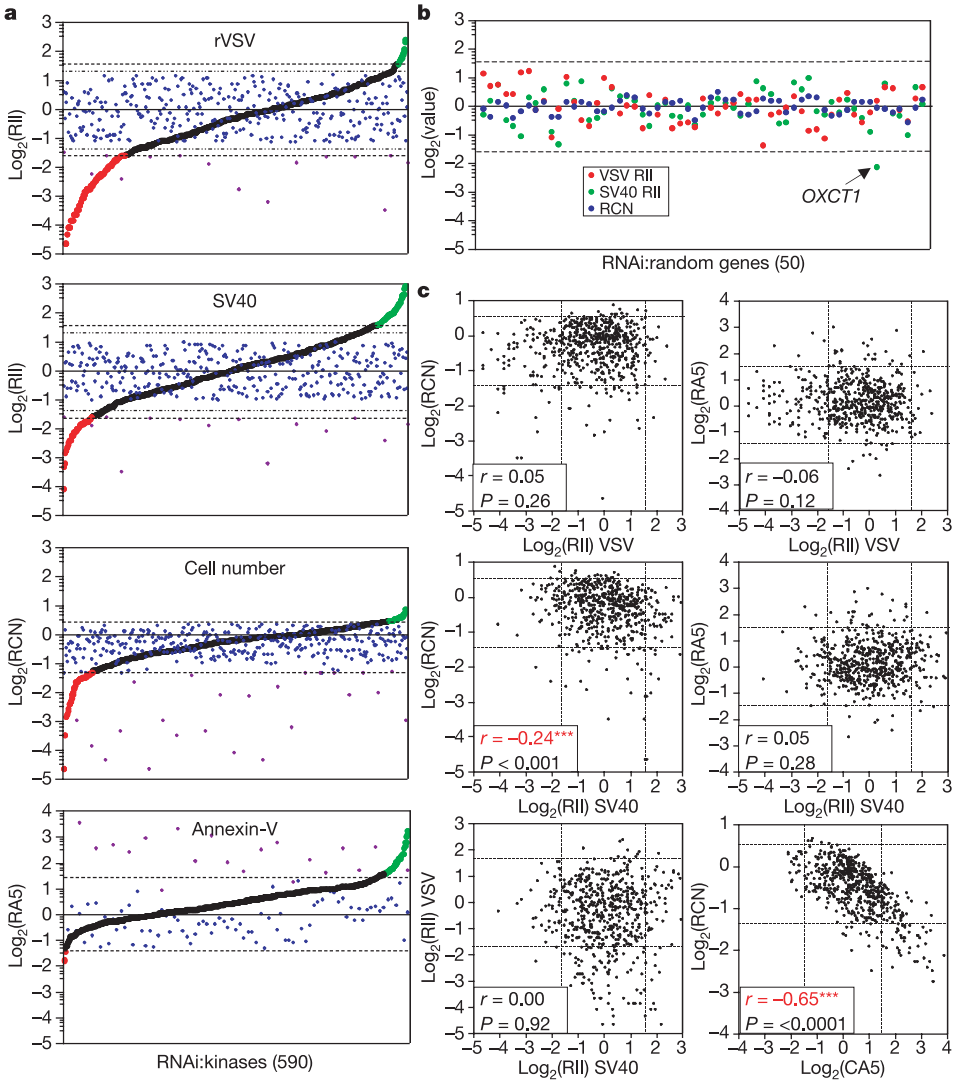


**Figure 1 | High-throughput, genome-wide analysis of human kinases involved in infectious virus entry (VSV or SV40), cell proliferation and cell death.** **a**, Average RII values, relative cell numbers (RCN) and relative Annexin-V staining (RA5), plotted on a $\log_2$ scale, of the silencing of 590 kinases in triplicate. Relative Annexin-V staining calculated as the ratio of the total Annexin-V-positive fluorescence signal in the sample to signal in negative control wells. Kinases with values <0.33 (RIIs) or <0.4 (RCN and RA5) are shown in red. Kinases with values >3 (RIIs), >1.5 (RCN) or >2.5 (RA5) shown in green. Kinases with RII, RCN or RA5 values falling between the threshold limits are shown in black. Negative controls shown in blue and positive controls in purple. Upper and lower dashed lines indicate scoring thresholds. **b**, Average RIIs and RCN (from triplicate samples) after silencing 50 randomly selected genes. Only one significant, SV40-specific hit (*OXCT1*; RII = 0.23 ± 0.11) was observed. **c**, Correlation analysis between RII, RCN and RA5 values. Values are plotted as $\text{Log}_2$, dashed lines indicate scoring thresholds, and boxes show Spearman *r* and *P* values (two-tailed tests). A low but significant negative correlation (statistical significance indicated by asterisks) between SV40 and RCN was found, and an expected, strong negative correlation was observed between RCN and RA5.

proliferation and induced cell death and cytotoxicity (not shown), there was no positive correlation with virus infection. Quite the opposite was found for SV40, in that genes required for cell proliferation were suppressors of infection and vice versa, suggesting that the hits did not generally reflect toxicity or cell death. Fourth, more than 80% of the hits were pathway-specific. 92 kinases scored in VSV infection, 80 in SV40 infection, and of the 36 affecting both VSV and SV40 infection, 23 gave inverse phenotypes, enhancing one pathway at the expense of the other.

### Virus entry phenotypes include endocytosis phenotypes

Because our primary assays measure translation of an early-transcribed viral gene, some of the kinases identified could potentially be involved in virus-specific, post-endocytic events, including

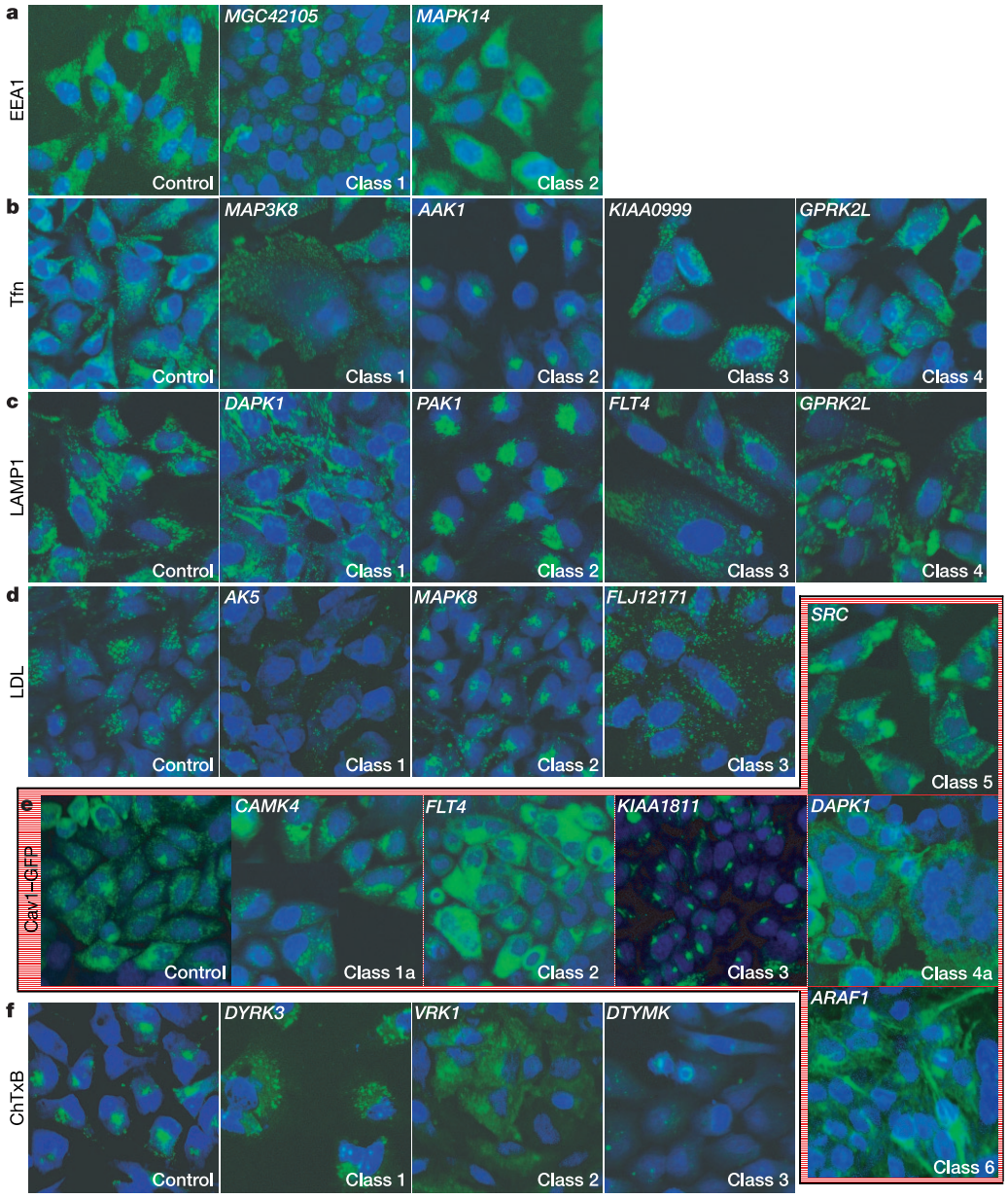


**Figure 2** | **Phenotypic profiling.** **a**–**f**, Representative images of phenotype classes are shown. Phenotypes are a result of the silencing of the indicated kinase. Nuclei are pseudocoloured blue, endocytic staining is green. **a**, EEA1 immunostaining. Class 1, large vacuolar structures; Class 2, diffuse cytosolic staining. **b**, Fluorescent Tfn uptake (10 min). Class 1, accumulation in small spots in the cell periphery; Class 2, strong accumulation in the perinuclear area; Class 3, accumulation in enlarged cytoplasmic structures; Class 4, polarized accumulation in plasma membrane protrusions. **c**, LAMP1 immunostaining. Class 1, structures aligning at the plasma membrane; Class 2, strong and condensed perinuclear accumulation; Class 3, distribution of structures throughout the cytoplasm; Class 4, polarized accumulation in plasma membrane protrusions. **d**, Fluorescent LDL uptake (30 min). Class 1, strongly reduced signal, accumulated in structures distributed throughout the cytoplasm; Class 2, strong and condensed perinuclear accumulation; Class 3, accumulation in vesicular structures throughout the cell. **e**, Cav1–GFP staining (images highlighted in pink). Class 1, signal in vesicular structures distributed throughout the cell (Class 1a) or more perinuclear (Class 1b, not shown); Class 2, diffuse staining distributed over the whole cell; Class 3, accumulation in a condensed perinuclear spot; Class 4, small punctuate structures and diffuse staining distributed on the cell surface (Class 4a) or in straight lines at the cell surface (Class 4b, not shown); Class 5, accumulation in peripheral foci; Class 6, diffuse surface staining and intracellular tubules. **f**, Fluorescent ChTxB uptake (60 min). Class 1, accumulation in vesicular structures distributed throughout the cytosol; Class 2, peripheral and diffuse staining; Class 3, strongly reduced signal.

NATURE 3571—6/5/2005—VBICKNELL—148660

synthesis and delivery of virus receptors, and transcription/translation of viral DNA/RNA. To validate the role of kinases in endocytosis, we applied secondary, high-content assays using an automated, high-throughput spinning disk confocal microscope (see Methods). First, we re-screened the complete kinome for fluorescent transferrin (Tfn) uptake and trafficking, and monitored four different phenotypic classes (Tfn Classes 1–4; see Fig. 2 and Supplementary Table S1). For a subset of 50 kinases (selected for their inverse phenotypes or unknown function), we monitored an additional 18 phenotypic classes for the two endocytic routes (Fig. 2). These included the morphology and distribution of cargo in the early endosome (stained using antibodies against EEA1) and late endosome (using antibodies against lysosomal antigen marker protein 1 or LAMP1), the distribution and morphology of caveolin-1–GFP (Cav1–GFP)-positive structures, trafficking of cargo to late endosomes (using fluorescent low density lipoprotein, LDL), and trafficking of cargo by caveolae/raft-mediated endocytosis (using fluorescent cholera toxin B, ChTxB) (Fig. 2 and Supplementary Table S3).

This phenotypic profiling verified that at least 72% of kinases affecting VSV infection (92/128) also played a role in CME, and that 87% of the phenotypically profiled kinases involved in SV40 infection (34/39) yielded perturbations in caveolae/raft trafficking. By extrapolation, the majority of kinases identified in the primary virus infection screens are thus predicted to be involved in endocytic trafficking. The secondary assays also confirmed that the two endocytic routes are differentially regulated: 21% (27/129) of the kinases acting in CME affected SV40 infection, and none of the kinases involved in caveolae/raft-mediated endocytosis affected VSV infection.

To order the kinases into a functional pattern, we performed a two-step cluster analysis[29] (Supplementary Table S3). First, hierarchical clustering was performed on the VSV/SV40 RIIs, differentiating ten groups of kinases with highly correlating phenotypes (Fig. 3, Groups 1–10). Second, within each group, kinases were clustered according to the RIIs and all phenotypic classes of the endocytic routes shown in Fig. 2 (Fig. 3). In addition, we manually annotated structural properties and previously ascribed functions (Supplementary Table S3 and references therein), and hierarchically clustered those kinases with well-established functions within

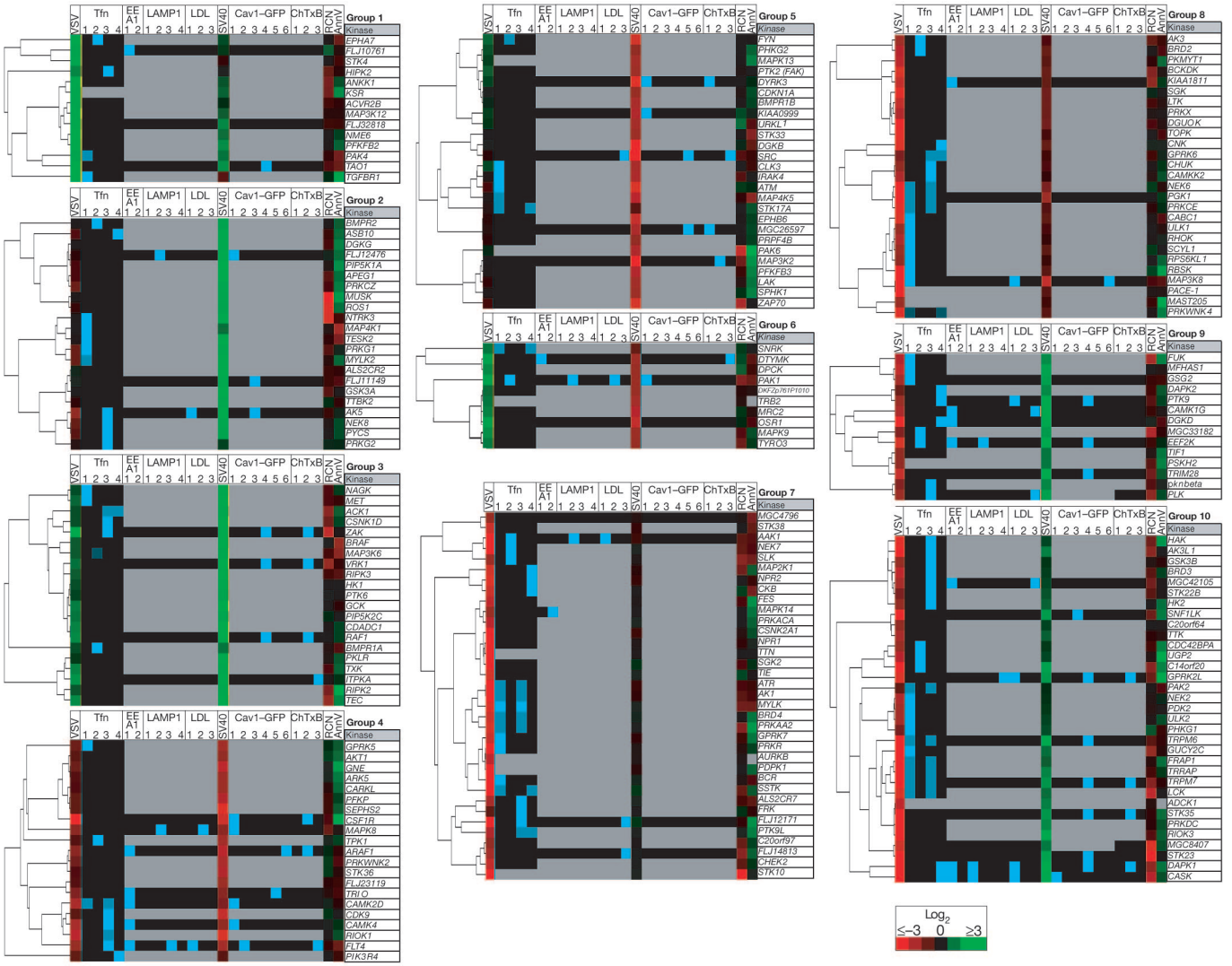


**Figure 3 | Hierarchical two-step clustering of RIIs and phenotypic profiles.** For a full explanation, see Supplementary Table S3. First, the SV40 and VSV RIIs were hierarchically clustered[29]. Ten groups that clustered strongly (>0.9) were identified. Next, the RIIs, RCN, RA5 and phenotypic profiles (according to the Classes outlined in Fig. 2) of the kinases were hierarchically clustered within each group, resulting in the depicted list of kinases. For the manual annotation of previously ascribed functions for each kinase, see Supplementary Table S3. NCBI URLs for each kinase are listed in Supplementary Table S1.

these different functional groups (Fig. 4). Cumulatively, the results revealed the existence of interconnected functional groups, as illustrated in the following examples.

### Regulation by metabolic kinases

Silencing of kinases regulating metabolic pathways might be expected to yield unspecific effects. Notably, 17 metabolic kinases scored specifically in VSV and 14 in SV40 infection. This specificity might in part reflect the need for specific lipids or glycans in both endocytic pathways. For example, *GNE* (Fig. 3, Group 4) regulates the production of sialic acid, which is required for biosynthesis of the SV40 receptor GM1 (ref. 26), and silencing of *GNE* specifically reduced SV40 infection. Knock-down of *FLJ12171* (also known as *FN3KRP*; Fig. 3, Group 7), a kinase that removes fructosamines from proteins, specifically blocked VSV infection and resulted in Tfn accumulation in enlarged endosomes (Tfn Class 3). This suggests unexpected regulatory functions of fructosamine modifications in the early endocytic pathway.

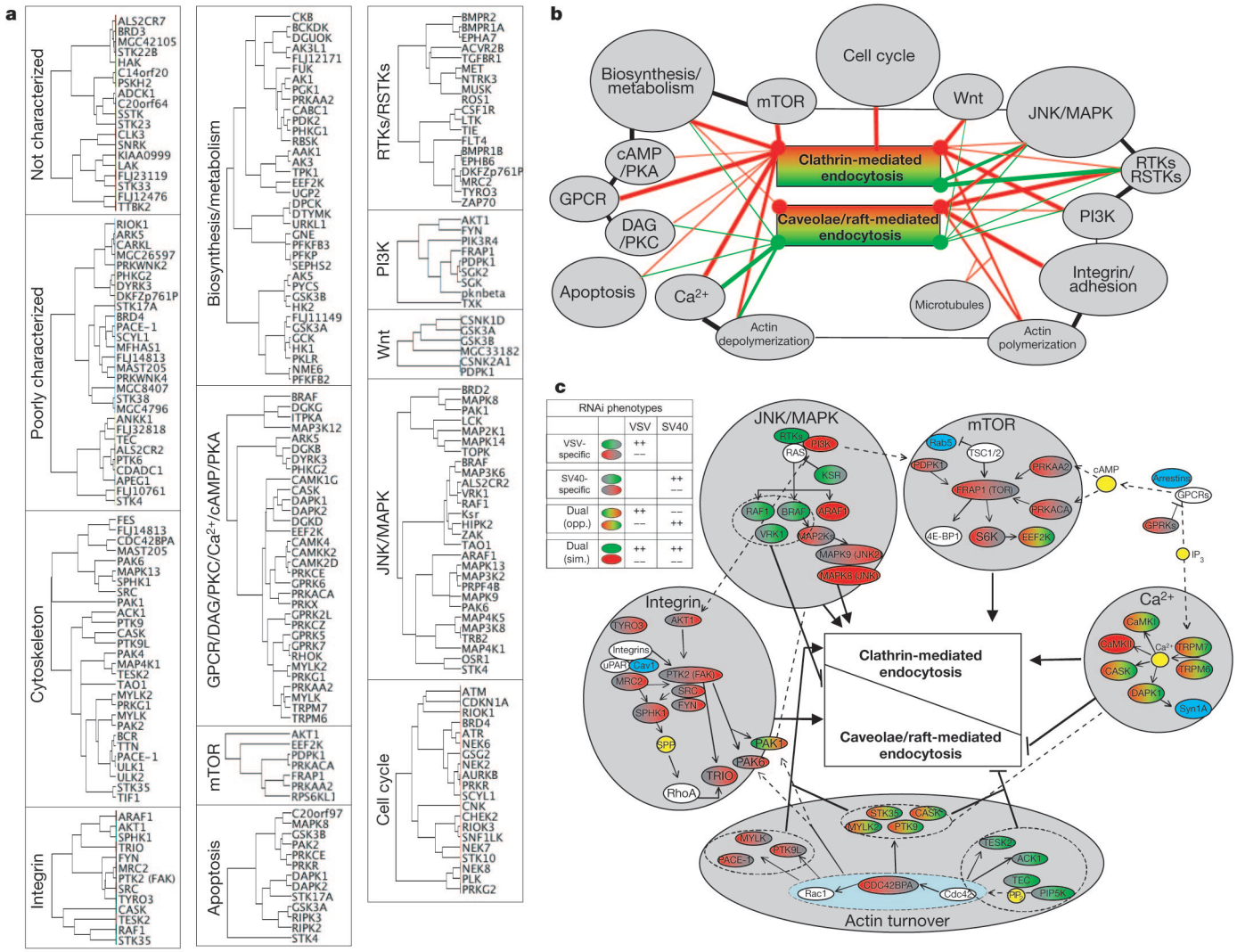


**Figure 4 | Effects of signalling pathways on endocytosis.** **a**, Using the previously ascribed functions (see Supplementary Table S2), kinases were assigned to 11 groups, in a non-exclusive manner: (1) not characterized at all, (2) poorly characterized, or involved in (3) regulation of the cytoskeleton, (4) integrin signalling and adhesion, (5) biosynthesis and metabolism, (6) GPCR signalling cascades involving DAG, $Ca^{2+}$ and cAMP, and the kinases PKC and PKA, (7) mTOR signalling, (8) apoptosis, (9) signalling from RTKs and RSTKs, (10) kinases functionally linked to PI(3)K, (11) the Wnt signalling pathway, (12) the JNK/MAPK cascade, and (13) the cell cycle. Kinases were then phenotypically clustered within each group (see Supplementary Fig. S2). **b**, The general effects on each endocytic route of the functional groups (see Supplementary Fig. S2) were deduced and indicated by coloured lines. Note that the colour code corresponds to the RNAi phenotype of a particular kinase. Red indicates that a kinase is required or is an activator of the pathway, and green indicates a kinase that is a suppressor of the endocytic pathway. **c**, Four representative examples of highly interconnected signalling networks. The TOR pathway regulating cell growth in response to nutrients specifically maintains or even stimulates CME. The integrin-signalling cascade, which controls focal adhesion assembly and turnover, is specifically required to activate or maintain caveolae/raft-mediated endocytosis. $Ca^{2+}$/calmodulin-dependent signalling and actin turnover orchestrated by Cdc42/Rac1 are two interconnected systems that exert opposite effects on the endocytic routes, suppressing caveolae/raft-mediated endocytosis while sustaining CME. A more complex regulatory activity is observed for the stress-induced and mitogenic signalling (JNK/MAPK) cascades, which can exert positive as well as negative effects on both endocytic routes. There are also connections between endocytosis and the cell cycle as well as programmed cell death. The phenotypes of the individual kinases are indicated by colours and by the position of that colour within the kinase symbol (colour on the left, VSV phenotype; colour on the right, SV40 phenotype). Generalized effects of networks on the endocytic routes are indicated with black arrows (required or activating) or black inhibitory symbols (suppressing).

NATURE 3571—6/5/2005—VBICKNELL—148660

### VSV infection and CME

Of the 80 kinases for which silencing strongly blocked VSV infection with little effect on SV40 infection (Fig. 3, Groups 7 and 8), 48 acted at different stages of the endocytic pathway. Phenotypes were observed in uptake, recycling and degradative transport. For example, silencing of *SSTK* (also called *TSSK6*) a Ser/Thr kinase with unknown function, inhibited internalization of Tfn (Tfn Class 1). Silencing of *AAK1*, which negatively regulates transferrin endocytosis, increased transport and accumulation of Tfn in perinuclear endosomes (Tfn Class 2), but also reduced VSV infection and uptake of low-density lipoprotein (LDL) (LDL Class 1).

**Regulation by TOR-dependent signalling.** Tor2p has been shown to regulate α-mating-factor receptor endocytosis in *S. cerevisiae*. Silencing of *FRAP1* (mammalian TOR) and five members of the TOR signalling pathway (*PDPK1*, *PRKAA2*, *PRKACA*, *RPS6KL1*, *EEF2K*) (Fig. 3, Groups 7–10 and Fig. 4) specifically blocked VSV infection, Tfn internalization (*RPS6KL1*, Tfn Class 1), intracellular trafficking (*PRKAA2*, *FRAP1*, Tfn Class 1 and 3), or recycling (*EEF2K*, Tfn Class 2). This shows that the nutrient-dependent TOR signalling pathway not only regulates ligand uptake but also imposes control at multiple steps of the CME pathway in human cells.

**Regulation by G-protein receptor-linked kinases.** Phosphorylation of G-protein-coupled receptors (GPCRs) by G-protein receptor-linked kinases (GPRKs) leads to their arrestin-dependent down-regulation by CME. We found that silencing of four different GPRKs expressed in HeLa cells (*GPRK5*, *GPRK6*, *GPRK7* and *RHOK*/*GRK1*) specifically reduced VSV infection and Tfn internalization (Tfn Class 1 and 4). GPRKs can therefore exert a more general form of control over CME, beyond the internalization of GPCRs.

**Cytoskeleton-dependent transport and cell polarity.** Our screen assigned a prominent role in endocytosis to a number of regulators of both the actin and tubulin cytoskeleton. Silencing of *MYLK* (Fig. 3, Group 7), which phosphorylates myosin light chain, caused an early block in Tfn uptake (Tfn Class 1 and 3). Silencing of *FLJ14813* (also called *MASTL*), a microtubule-associated Ser/Thr (MAST)-like kinase, reduced the accumulation of LDL in perinuclear structures (LDL Class 3), suggesting that it is required for late endocytic transport.

Ablation of *PTK9L* (Fig. 3, Group 7), which binds monomeric actin and can be phosphorylated by c-Src, CK2 (*CSNK2A1*, see below) and PKCζ (*PRKCZ*), resulted in redistribution of Tfn-positive vesicles to membrane protrusions and lamellae (Tfn Class 3 and 4). PKCζ, which regulates cell polarization, might therefore re-programme the activity and distribution of the recycling system via *PTK9L*. Silencing of *ULK1* and *ULK2* blocked Tfn internalization (Tfn Class 1) (Fig. 3, Groups 7, 8 and 10). Both of these kinases are homologous to *C. elegans* Unc51.1, which binds to microtubules, regulates Rab5-dependent endocytic transport[30] (as part of a complex with SynGAP and syntenin), and is involved in axonal elongation.

### SV40 infection and caveolae/raft-mediated endocytosis

Because SV40 can use caveolae-mediated endocytosis, as well as a very related (if not identical) uptake route internalizing lipid rafts in the absence of Cav1 (ref. 18), the kinases we identified as affecting SV40 infection might be involved in both endocytic routes. Indeed, silencing of ten kinases in HeLa cells conditionally depleted for Cav1 by RNAi affected SV40 infection as in control cells (Supplementary Fig. S1b). These data suggest that this group of kinases also function in caveolae-independent, raft-dependent endocytosis, acting as regulators of this enigmatic transport route.

Among the 43 kinases specifically required for SV40 infection, we detected a series of interesting phenotypes to do with caveolae trafficking. For example, silencing of *KIAA0999* (*FLJ12240*), an unknown Ser/Thr kinase, and *DYRK3*, a MAPK-related kinase involved in cell growth and survival (Fig. 3, Group 5), caused a redistribution of green fluorescent protein (GFP)-labelled Cav1 and internalized ChTxB to enlarged vesicular structures (ChTxB Class 1). We also observed clustering of caveolae at peripheral foci (Cav1–GFP Class 5), tubulation of intracellular Cav1–GFP-positive structures (Cav1–GFP Class 6), and diffuse cell-surface staining (Cav1–GFP Class 4) (Fig. 2). Using quantitative total internal reflection fluorescence microscopy, we could show a specific role for kinases at different stages of the caveolar assembly and transport cycle[31].

**Regulation by focal adhesion and integrin signalling.** SV40 infection was specifically reduced by silencing of (1) *PTK2*/*FAK* and *SRC* (Fig. 3, Group 5), which regulate integrin-dependent focal adhesion assembly and turnover, (2) *MRC2*, a collagen receptor tyrosine kinase, and (3) several other members of cell adhesion-dependent signalling (*FYN*, *AKT1*, *TYRO3*, *PAK6* and *SPHK1*, Fig. 3). The clustering of Cav1–GFP-positive and ChTxB-positive structures at peripheral foci (Cav1-GFP Class 5) seen after silencing of *SRC* and *MGC26597* (a predicted protein with potential phosphatidylinositol-4-phosphate-5-kinase, PI(4,5)K activity), suggests that these kinases regulate caveolae/raft-mediated traffic to, and from, focal adhesions, supporting the idea that the extracellular matrix can modulate this trafficking route[32,33].

**Cdc42-mediated suppression of endocytosis.** As a prerequisite to internalization by caveolae, SV40 is thought to stimulate a cycle of cortical actin depolymerization and polymerization[34]. Interestingly, among the hits that specifically enhanced SV40 infection were two PI(4,5)Ks (*PIP5K1A*, *PIP5K2C*), a PH-domain-containing Src-family kinase (*TEC*) that activates Cdc42 and actin polymerization, and two Cdc42 effectors, *ACK1*/*TNK2* and *TESK2*, which enhance actin polymerization. These data suggest that caveolae/raft-mediated endocytosis is suppressed by the stabilizing effect that Cdc42- and PI(4,5)$P_2$-dependent signalling have on cortical actin. However, as *MGC26597* is required for SV40 infection, different PI(4,5)Ks might regulate the actin cycle and exert opposite effects on this endocytic route.

### Coordination between endocytic pathways

Among the 36 kinases found to have a role in both VSV and SV40 infection, a subset (23 kinases) exerted opposite effects on the two virus entry mechanisms. For those kinases for which silencing inhibited VSV infection and enhanced SV40 infection (Fig. 3, Groups 9 and 10), phenotypic profiling revealed a functional association with transport to late endosomes. For example, knockdown of two $Ca^{2+}$ channels with kinase domains (*TRPM6*, *TRPM7*) inhibited VSV infection and stimulated SV40 infection. Similar effects were observed for several $Ca^{2+}$/calmodulin-activated kinases (for example, *CASK*, *DAPK1*, *DAPK2*, *DGKD*), silencing of which caused early or late endosomes to accumulate underneath the cell surface. The concomitant enhancement of SV40 infection suggests either that caveolae/raft-mediated endocytosis compensates for reduced CME, or that cargo internalized by caveolae bypasses the endosomes, leading to increased transport of SV40 to the ER and enhancing infection[28].

**Actin cytoskeleton.** Among the kinases coordinating the two endocytic routes were effectors of Cdc42 and Rac1, implicated in the regulation of the actin cytoskeleton (see above). Their activity in endocytosis correlated with the intracellular distribution of endosomes, as shown by the opposite effects of *PTK9* and *PAK1*. Silencing of *PTK9* (twinfilin), which binds monomeric actin and is targeted by Cdc42 and Rac1 to regions of high actin turnover, inhibited VSV and enhanced SV40 infection, and redistributed endocytic organelles to the cell periphery. Conversely, depletion of the p21-activated kinase *PAK1*, an effector of Cdc42 and Rac1 that depolymerizes actin, increased VSV infection, reduced SV40 infection, and induced the clustering of endocytic organelles in the perinuclear region.

**Wnt/β-catenin signalling.** Silencing of two glycogen synthase kinases (*GSK3A* and *GSK3B*) and three casein kinases (*CSNK1D*, *MGC33182*/*CSNK1A1L* and *CSNK2A1*), all known to signal for proteasomal degradation of β-catenin in the absence of Wnt ligand,

reduced VSV and enhanced SV40 infection. Notably, ablation of *GSK3B* and *CSNK1D* resulted in accumulation of Tfn in early endosomes (Class 3), suggesting that β-catenin degradation is regulated by the same kinases that control endocytic downregulation of cell-surface components (for example, cadherins).

**Mitogenic and other signalling pathways.** Our comparative analysis of phenotypes in clathrin- versus caveolar/raft-dependent pathways, cell growth, proliferation and apoptosis has provided an integrated view of signalling and endocytosis. The screen identified pro-apoptotic kinases (for example, Death-associated protein kinase 1 DAPK1), the ablation of which yielded an endocytic phenotype (Fig. 4). One surprise was the extent to which the mitogenic signalling cascade participates in endocytosis (Fig. 4): nine receptor tyrosine kinases (RTKs) and four receptor Ser/Thr kinases (RSTKs) expressed in HeLa cells were either required for (four for SV40, none for VSV infection alone, two for both SV40 and VSV infection) or suppressed (five for SV40 and three for VSV infection) the virus infectious entry routes. In addition, we identified at least 28 kinases of the mitogenic signalling/JNK cascade[35–37] with a variety of different phenotypic classes. Among the silencing phenotypes of the 37 suppressors of SV40 infection (Fig. 3, Group 3, for example, *ZAK*, *VRK1* and *RAF1*), we frequently observed diffuse or fine, punctuate staining of Cav1–GFP in the periphery of the cell (Cav1–GFP Class 4), with ChTxB accumulating in enlarged intracellular vesicles (ChTxB Class 2).

As CME and endosome fusion are arrested during mitosis[38,39], we were not surprised to see the screen identify kinases regulating cell-cycle progression (Fig. 4). Silencing of *MAP2K1* (*MEK1*) and *CNK* (also *PLK3* or Polo-like kinase-3), known to fragment the Golgi during the cell cycle, re-targeted Tfn-containing endosomes to plasma membrane protrusions (Tfn Class 4), suggesting that this signalling cascade also regulates the distribution of recycling endosomes. This mechanism might serve to partition endosomes between daughter cells or supply membranes to the cleavage furrow during cytokinesis.

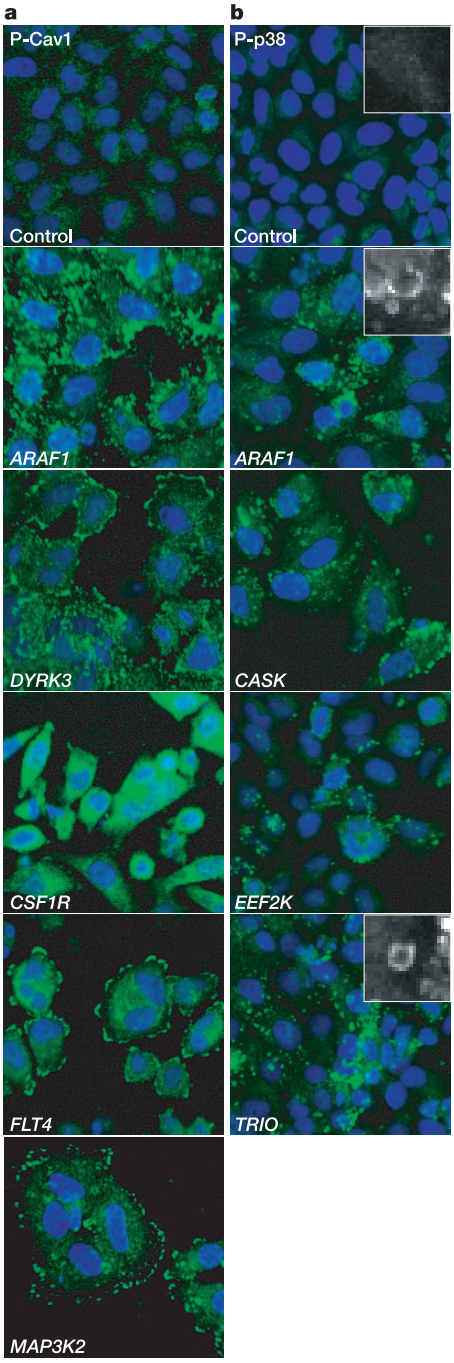


**Figure 5 | Phosphorylation of Cav1 and p38 MAPK. a**, HeLa cells silenced for the indicated kinases were fixed and stained with a monoclonal antibody against caveolin-1 phosphorylated on Tyr 14 (P-Cav1). In control cells, some P-Cav1 is detected but the level is low. Silencing of the indicated kinases induces hyperphosphorylation and location-specific phosphorylation of Cav1. **b**, HeLa cells silenced for the indicated kinases were fixed and stained with a monoclonal antibody against phosphorylated p38 (P-p38). In control cells, low levels of phosphorylated p38 are detected. Silencing of the indicated kinases induces hyperphosphorylation of P-p38, which is then detected on intracellular, enlarged endosome-like structures (see insets).

## Changes in Cav1 and MAPK p38 phosphorylation

To explore the function of kinases on the target endocytic machinery, we inspected the phosphorylation of Cav1 because it has been suggested to regulate endocytosis of caveolae/lipid rafts[40,41]. Unexpectedly, we detected increased levels of phosphorylated Cav1 and changes in localization upon silencing of several kinases required for SV40 infection (Fig. 5a). Because silencing of *ARAF*/*ARAF1* and *DYRK3* also modified the cellular distribution of Cav1–GFP (Cav1–GFP Class 1 and 6), coat stability and dynamics of caveolae on the cell surface[31], our data suggest that, in addition to Cav1 phosphorylation, a network of kinases positively and negatively regulates the dynamics and transport activity of caveolae.

We observed cytosolic staining of EEA1 (EEA1 Class 2) upon silencing of the stress-activated kinase *MAPK14* (p38β; Fig. 2). Like JNK, p38 MAPK lies at the centre of stress-induced signalling cascades[37] and regulates endocytosis by phosphorylating components of the endocytic machinery[42,51]. We tested whether kinases regulating CME could act through phosphorylation of p38. Phosphorylated p38 was low in non-stimulated cells, but increased upon silencing of several kinases required for VSV infection (Fig. 5b). Concomitantly, and although the non-phosphorylated kinase is mainly cytosolic[42], phosphorylated p38 associated with enlarged endosomes (Fig. 5b). Thus, ablation of various kinases mimics the stress-induced activation of p38 MAPK[37] resulting in recruitment of phosphorylated p38 to endosomes and modulation of endocytosis.

## Discussion

Since the initial observations that kinases regulate endocytosis[43], a more general appreciation of their role at distinct steps of the endocytic pathway has been lacking[1]. Our genome-wide screen fills this gap by contributing a comprehensive analysis of the involvement of human kinases in two endocytic routes. For example, the identification of new kinases regulating the stability of the caveolar coat and caveolae dynamics provides long-sought-after regulators of this transport route[31]. Furthermore, our screen reveals some new design principles governing endocytosis. First, we identified an unexpected number of kinases (210) involved in endocytosis, several of which

(47) were poorly characterized or uncharacterized. Although not all kinases would be expected to play a direct mechanistic role in endocytosis (see below), we observed high selectivity for one of the two endocytic routes, even for regulators of metabolic functions. Second, the finding that some kinases can positively affect one endocytic route at the expense of of the other suggests that clathrin- and caveolae-mediated endocytosis are coordinated to ensure a proper balance in membrane homeostasis and signalling activities. Third, a large group of the kinases identified in our endocytosis screen also function in various signalling pathways, strengthening the emerging paradigm that endocytic transport and signal transduction are tightly coupled. This might in part explain the complexity observed, in that only some kinases within a given signalling network act directly upon the endocytic machinery, with the majority having only a modulatory role. A generalization of the higher-order control of signalling cascades on the endocytic pathway is depicted in Fig. 4a, b. Depending on the signalling system, kinases entrain the endocytic machinery to respond with either clathrin- or caveolae/raft-dependent endocytosis, or both. It appears that endocytosis is subjected to regulatory control by the signalling machinery even under normal growth conditions. For example, our data and others[51] argue for a role of the stress-response p38MAPK[42] in endocytosis also under physiological conditions.

These observations form a framework for rethinking how cells respond and adapt to different stimuli. Endocytosis has a much wider role than downregulating activated growth factor–receptor complexes[44–47], by providing spatio-temporal regulation to the signalling response. First, growth factor–receptor complexes can modify their own intracellular itinerary, by activating downstream kinase cascades. For example, four mitogenic kinases suppress caveolae/raft-mediated endocytosis by regulating Cav1 phosphorylation. As caveolae keep signalling molecules in an inhibited state[48], this feedback mechanism might be universally applied in controlling cell proliferation: A significant correlation across the kinome (Fig. 2c) indicates that kinases required for cell proliferation tend to suppress caveolae/raft-mediated endocytosis, whereas inhibitory kinases have the opposite effect. In addition to these general considerations, the endocytic response to kinases clearly also depends on the cell type. Second, by regulating the motility of endosomes along the cytoskeleton, kinases might enable signalling molecules on endosomes to propagate signals from the plasma membrane to the nucleus by direct transport rather than simple diffusion[49]. Our findings have also implications for biomedical research and drug development, through the identification of new mechanisms of action and potential therapeutic targets. Finally, by extending our high-throughput analysis to the entire human genome, we will eventually be able to obtain a functional genetic map of endocytic pathways. The challenge then will be to translate this framework into a quantitative model that incorporates parameters including transport kinetics, changes in morphology and localization, and response magnitude, and can predict responses under different physiological conditions.

## METHODS

**siRNA design and silencing efficiency.** Three unique sites within the coding sequence of each human kinase were selected (Cenix Bioscience GmbH), 21-mer oligonucleotides synthesized (Ambion Inc.) and gene silencing potential verified by real-time polymerase chain reaction (PCR). The most potent 21-mers (resulting in >70% reduction of mRNA levels after 3 days) were included in the kinase siRNA library. Re-screening of 50 kinases using the VSV and SV40 infectious entry assays with independent siRNA sequences resulted in the same phenotype in 48/50 (SV40) and 50/50 cases (VSV).

**High-throughput siRNA screening of infectious virus entry.** rVSV–GFP and SV40 (strain 776) were prepared according to published protocols[17,50]. Between cell plating and fixation, no washing steps were required. HeLa cells (4,000 per well) were plated in 80 μl of complete medium in 96-well plates and incubated at 37 °C and 5% $CO_2$. The next day, 1 μl of 10 μM siRNA, diluted in 16 μl of Optimem with 0.4 μl oligofectamine in 2.6 μl Optimem, was added directly to the cells and incubated for 3 days. After 3 days, cells were incubated for 3 h with rVSV–GFP or for 36 h with SV40 at 37 °C and 5% $CO_2$. After infection, cells were fixed with paraformaldehyde (PFA), permeabilized with Triton X-100 (TX100) and stained with 4,6-diamidino-2-phenylindole (DAPI). A monoclonal antibody directly conjugated to Alexa Fluor 488 (AF488) was used to detect SV40 large T-antigen expression. In separate plates, gene-silenced, PFA-fixed and BSA-blocked cells were stained with 1 μg ml$^{-1}$ AF488-Annexin-V for 1 h in PBS.

**Automated imaging and quantification.** In a fully automated and double-blind manner, five images were taken per well, the total number of cells (DAPI) and infected cells (GFP/AF488) per well calculated, and average and standard deviations for triplicate experiments determined. These were used to calculate RII, relative cell number (RCN) and relative Annexin-V staining (RA5) (Fig. 1). For determination of the signal noise, numbers obtained from each field of control-treated cells were not averaged, but regarded as individual measurements of the noise spectrum.

**High-content endocytosis assays.** Fixed and permeabilized cells were stained with anti-EEA1 or -LAMP1 antibodies (BD Biosciences Pharmingen) and appropriate secondary antibodies. Cav1 distribution was studied in siRNA-treated HeLa cells stably expressing Cav1–GFP[28]. For ligand trafficking, siRNA-treated HeLa cells were incubated in 1 μg ml$^{-1}$ AF488-Tfn for 10 min, 1 μg ml$^{-1}$ DiI-LDL for 30 min, and 1 ng ml$^{-1}$ AF488-ChTxB for 60 min. Cells were washed, fixed and stained with DRAQ5 (Alexis Biochemicals) to visualize nuclei. The Opera automated spinning-disk confocal microscope (Evotec Technologies GmbH) was used to image 96-well plates, using 488-nm, 532-nm and 633-nm laser lines and a water-immersion 20 × objective with a numerical aperture of 1.2. Twenty fields per well (each containing ~100 cells under control conditions) were imaged and experiments were performed in triplicate. Images were analysed manually and phenotypes scored when appearing in at least five fields in each triplicate.

**Hierarchical clustering.** The phenotypic classes were first converted into a numerical representation: The value 1.000 ($2^0$) was assigned to all samples with no phenotypes, and the value 0.125 ($2^{-3}$) to the phenotype observed. If two phenotypes were observed within one assay (for example, Tfn Class 1 and 3), each phenotype was given the value 0.250 ($2^{-2}$). In a few cases where the phenotype was less penetrant, it was given the value 0.500 ($2^{-1}$). For Fig. 3, the RII values were loaded into Cluster 3.0, $\log_2$-transformed and hierarchically clustered using uncentred correlation and centroid linkage[29], yielding ten infection-phenotype groups of kinases clustering >0.9. Next, the RII, RCN, RA5 and phenotypic profiling values were loaded into Cluster 3.0 by infection-phenotype group, and processed as above. In Fig. 3, 11 functional groups were assembled on the basis of functions previously ascribed to the kinases. Next, the RII, RCN, RA5 and phenotypic profiling values were loaded into Cluster 3.0 by functional group, and processed as above. Java TreeView was used to make cluster trees and graphic displays of the phenotypes.

**Received 28 January; accepted 17 March 2005**
**Published online 11 May 2005.**

1. Conner, S. D. & Schmid, S. L. Regulated portals of entry into the cell. *Nature* **422,** 37–44 (2003).
2. Di Fiore, P. P. & De Camilli, P. Endocytosis and signaling. an inseparable partnership. *Cell* **106,** 1–4 (2001).
3. Gonzalez-Gaitan, M. Signal dispersal and transduction through the endocytic pathway. *Nature Rev. Mol. Cell Biol.* **4,** 213–224 (2003).
4. Miaczynska, M., Pelkmans, L. & Zerial, M. Not just a sink: endosomes in control of signal transduction. *Curr. Opin. Cell Biol.* **16,** 400–406 (2004).
5. Carpenter, A. E. & Sabatini, D. M. Systematic genome-wide screens of gene function. *Nature Rev. Genet.* **5,** 11–22 (2004).
6. Manning, G., Whyte, D. B., Martinez, R., Hunter, T. & Sudarsanam, S. The protein kinase complement of the human genome. *Science* **298,** 1912–1934 (2002).
7. Lucocq, J., Warren, G. & Pryde, J. Okadaic acid induces Golgi apparatus fragmentation and arrest of intracellular transport. *J. Cell Sci.* **100,** 753–759 (1991).
8. Simonsen, A., Wurmser, A. E., Emr, S. D. & Stenmark, H. The role of phosphoinositides in membrane transport. *Curr. Opin. Cell Biol.* **13,** 485–492 (2001).
9. Nguyen, C. & Bibb, J. A. Cdk5 and the mystery of synaptic vesicle endocytosis. *J. Cell Biol.* **163,** 697–699 (2003).
10. Mellman, I. Endocytosis and molecular sorting. *Annu. Rev. Cell Dev. Biol.* **12,** 575–625 (1996).
11. Helenius, A., Kartenbeck, J., Simons, K. & Fries, E. On the entry of Semliki forest virus into BHK-21 cells. *J. Cell Biol.* **84,** 404–420 (1980).
12. Smith, A. E. & Helenius, A. How viruses enter animal cells. *Science* **304,** 237–242 (2004).
13. Sieczkarski, S. B. & Whittaker, G. R. Differential requirements of rab5 and rab7 for endocytosis of influenza and other enveloped viruses. *Traffic* **4,** 333–343 (2003).

14. Kartenbeck, J., Stukenbrok, H. & Helenius, A. Endocytosis of simian virus 40 into the endoplasmic reticulum. *J. Cell Biol.* **109,** 2721–2729 (1989).
15. Anderson, H. A., Chen, Y. & Norkin, L. C. Bound simian virus 40 translocates to caveolin-enriched membrane domains, and its entry is inhibited by drugs that selectively disrupt caveolae. *Mol. Biol. Cell* **7,** 1825–1834 (1996).
16. Stang, E., Kartenbeck, J. & Parton, R. G. Major histocompatibility complex class I molecules mediate association of SV40 with caveolae. *Mol. Biol. Cell* **8,** 47–57 (1997).
17. Pelkmans, L., Kartenbeck, J. & Helenius, A. Caveolar endocytosis of simian virus 40 reveals a new two-step vesicular-transport pathway to the ER. *Nature Cell Biol.* **3,** 473–483 (2001).
18. Damm, E.-M. *et al.* Clathrin and caveolin-1 independent endocytosis: entry of simian virus 40 into cells devoid of caveolae. *J. Cell Biol.* **168,** 477–488 (2005).
19. Razani, B. & Lisanti, M. P. Caveolins and caveolae: molecular and functional relationships. *Exp. Cell Res.* **271,** 36–44 (2001).
20. Lu, Z., Ghosh, S., Wang, Z. & Hunter, T. Downregulation of caveolin-1 function by EGF leads to the loss of E-cadherin, increased transcriptional activity of β-catenin, and enhanced tumor cell invasion. *Cancer Cell* **4,** 499–515 (2003).
21. Di Guglielmo, G. M., Le Roy, C., Goodfellow, A. F. & Wrana, J. L. Distinct endocytic pathways regulate TGF-beta receptor signalling and turnover. *Nature Cell Biol.* **5,** 410–421 (2003).
22. Elbashir, S. M. *et al.* Duplexes of 21-nucleotide RNAs mediate RNA interference in cultured mammalian cells. *Nature* **411,** 494–498 (2001).
23. Kirchhausen, T. Clathrin. *Annu. Rev. Biochem.* **69,** 699–727 (2000).
24. Simonsen, A. *et al.* EEA1 links PI(3)K function to Rab5 regulation of endosome fusion. *Nature* **394,** 494–498 (1998).
25. Stahlhut, M. & van Deurs, B. Identification of filamin as a novel ligand for caveolin-1: evidence for the organization of caveolin-1-associated membrane domains by the actin cytoskeleton. *Mol. Biol. Cell* **11,** 325–337 (2000).
26. Tsai, B. *et al.* Gangliosides are receptors for murine polyoma virus and SV40. *EMBO J.* **22,** 4346–4355 (2003).
27. Rothman, J. E. Mechanisms of intracellular protein transport. *Nature* **372,** 55–63 (1994).
28. Pelkmans, L., Burli, T., Zerial, M. & Helenius, A. Caveolin-stabilized membrane domains as multifunctional transport and sorting devices in endocytic membrane traffic. *Cell* **118,** 767–780 (2004).
29. Eisen, M. B., Spellman, P. T., Brown, P. O. & Botstein, D. Cluster analysis and display of genome-wide expression patterns. *Proc. Natl Acad. Sci. USA* **95,** 14863–14868 (1998).
30. Zerial, M. & McBride, H. Rab proteins as membrane organizers. *Nature Rev. Mol. Cell Biol.* **2,** 107–117 (2001).
31. Pelkmans, L. & Zerial, M. Kinase-regulated quantal assemblies, kiss-and-run and recycling of caveolae. *Nature* (submitted).
32. Wary, K. K., Mariotti, A., Zurzolo, C. & Giancotti, F. G. A requirement for caveolin-1 and associated kinase Fyn in integrin signaling and anchorage-dependent cell growth. *Cell* **94,** 625–634 (1998).
33. del Pozo, M. A. *et al.* Integrins regulate Rac targeting by internalization of membrane domains. *Science* **303,** 839–842 (2004).
34. Pelkmans, L., Puntener, D. & Helenius, A. Local actin polymerization and dynamin recruitment in SV40-induced internalization of caveolae. *Science* **296,** 535–539 (2002).
35. Wellbrock, C., Karasarides, M. & Marais, R. The RAF proteins take centre stage. *Nature Rev. Mol. Cell Biol.* **5,** 875–885 (2004).
36. Schlessinger, J. Cell signaling by receptor tyrosine kinases. *Cell* **103,** 211–225 (2000).
37. Davis, R. J. Signal transduction by the JNK group of MAP kinases. *Cell* **103,** 239–252 (2000).
38. Warren, G., Davoust, J. & Cockcroft, A. Recycling of transferrin receptors in A431 cells is inhibited during mitosis. *EMBO J.* **3,** 2217–2225 (1984).
39. Tuomikoski, T., Felix, M. A., Doree, M. & Gruenberg, J. Inhibition of endocytic vesicle fusion *in vitro* by the cell-cycle control protein kinase cdc2. *Nature* **342,** 942–945 (1989).
40. Minshall, R. D., Sessa, W. C., Stan, R. V., Anderson, R. G. & Malik, A. B. Caveolin regulation of endothelial function. *Am. J. Physiol. Lung Cell. Mol. Physiol.* **285,** L1179–L1183 (2003).
41. Sharma, D. K. *et al.* Selective stimulation of caveolar endocytosis by glycosphingolipids and cholesterol. *Mol. Biol. Cell* **15,** 3114–3122 (2004).
42. Cavalli, V. *et al.* The stress-induced MAP kinase p38 regulates endocytic trafficking via the GDI:Rab5 complex. *Mol. Cell* **7,** 421–432 (2001).
43. Woodman, P. G., Mundy, D. I., Cohen, P. & Warren, G. Cell-free fusion of endocytic vesicles is regulated by phosphorylation. *J. Cell Biol.* **116,** 331–338 (1992).
44. Dubois, L., Lecourtois, M., Alexandre, C., Hirst, E. & Vincent, J. P. Regulated endocytic routing modulates wingless signaling in *Drosophila* embryos. *Cell* **105,** 613–624 (2001).
45. Xue, L. & Lucocq, J. ERK2 signalling from internalised epidermal growth factor receptor in broken A431 cells. *Cell. Signal.* **10,** 339–348 (1998).
46. Teis, D., Wunderlich, W. & Huber, L. A. Localization of the MP1–MAPK scaffold complex to endosomes is mediated by p14 and required for signal transduction. *Dev. Cell* **3,** 803–814 (2002).
47. Di Guglielmo, G. M., Baass, P. C., Ou, W. J., Posner, B. I. & Bergeron, J. J. Compartmentalization of SHC, GRB2 and mSOS, and hyperphosphorylation of Raf-1 by EGF but not insulin in liver parenchyma. *EMBO J.* **13,** 4269–4277 (1994).
48. Parton, R. G. Caveolae–from ultrastructure to molecular mechanisms. *Nature Rev. Mol. Cell Biol.* **4,** 162–167 (2003).
49. Kholodenko, B. N. Four-dimensional organization of protein kinase signaling cascades: the roles of diffusion, endocytosis and molecular motors. *J. Exp. Biol.* **206,** 2073–2082 (2003).
50. Schnell, M. J., Buonocore, L., Whitt, M. A. & Rose, J. K. The minimal conserved transcription stop-start signal promotes stable expression of a foreign gene in vesicular stomatitis virus. *J. Virol.* **70,** 2318–2323 (1996).
51. Macé, G., Miaczynska, M., Zerial, M. & Nebreda, A. R. Phosphorylation of EEAI by p38MAP kinase regulates m opioid receptor endocytosis. *EMBO J.* (submitted).

**Supplementary Information** is linked to the online version of the paper at www.nature.com/nature.

**Acknowledgements** We thank F. Halley and A. Kroenke for experimental assistance, J. Rose for rVSV, and G. Kochs for hybridomas expressing anti-Tag antibodies. I. Baines (Biopolis Dresden Consultants GmbH), D. Dorris (Ambion Inc.), C. Echeverri (Cenix Bioscience GmbH), R. Günther (Evotec Technologies GmbH) and M. Athelogou (Definiens AG) are acknowledged for making HT RNAi technologies and high-content, automated imaging and analysis technologies available. We thank F. Buchholz, C.-P. Heisenberg, M. Miaczynska, D. Meder, A. Schenck, A. Helenius and K. Simons for discussions and critical reading of the manuscript. L.P. would like to thank A. Helenius for continuous support. This work was supported by grants from the Max Planck Society 'RNAi interference' initiative and the Bundesministerium für Bildung und Forschung. L.P. is a Marie Curie fellow.

**Author Contributions** L.P. and M.Z. conceived the experimental idea. L.P. carried out the experiments with help from E.F., H.G. and M.H. Data analysis was carried out by L.P., B.H. and M.Z. L.P., E.K. and M.Z. together with I. Baines conceived and set up the HT-TDS and financed the project. L.P. and M.Z. wrote the manuscript.

**Author Information** Reprints and permissions information is available at npg.nature.com/reprintsandpermissions. The authors declare no competing financial interests. Correspondence and requests for materials should be addressed to M.Z. (zerial@mpi-cbg.de).